

Real-time full-field imaging through scattering media by all-optical feedback

Ronen Chriki , Simon Mahler *, Chene Tradonsky, Asher A. FrieSEM , and Nir Davidson
Department of Physics of Complex Systems, Weizmann Institute of Science, Rehovot 761001, Israel

 (Received 10 May 2021; accepted 23 February 2022; published 29 March 2022)

Full-field imaging through scattering media is fraught with many challenges. Despite many achievements, current imaging methods are too slow to deal with fast dynamics, e.g., in biomedical imaging. We present an ultrafast all-optical method where a highly multimode self-imaging laser cavity is built around the reflective object to be imaged and the scattering medium. We show that the intracavity laser light from the object is mainly focused onto specific regions of the scattering medium where the phase variations are low. Thus, round-trip loss within the laser cavity is minimized, thereby overcoming most of the scattering effects. Our method can deal with temporal variations that occur on timescales as short as several cavity round trips, typically 100 ns in our laser cavity.

DOI: [10.1103/PhysRevA.105.033527](https://doi.org/10.1103/PhysRevA.105.033527)

Optical imaging through scattering media, e.g., in biomedical imaging and imaging through atmospheric turbulence, is fraught with many difficulties. The complex structure of such media causes random variations in refractive index, such that an incoming beam is scattered and distorted. As a result, images are blurred or speckled when observed through scattering media [1,2]. Over the past decade, several interesting methods were developed to overcome these deleterious scattering effects, mainly by exploiting either spatial correlations of the seemingly random speckle pattern [3–6] or by shaping the wavefront of the incoming beam [7–10].

However, methods based on spatial correlations are mostly applicable to fluorescent objects, which typically have weak signals, and consequently require long integration time to obtain sufficient signal-to-noise ratio. Thus, they are only adequate for objects that remain stationary over long acquisition times. Methods based on wavefront shaping involve deformable mirrors or spatial light modulators that control the shape of the incoming wavefront to compensate for the effect of the scattering media. These methods usually require a bright reference “guidestar” and are based on iterative time-consuming computer algorithms, typically lasting several seconds or more. During the extensive time period needed to shape the incoming wavefront, the object cannot evolve and must remain steady on a scale smaller than a wavelength. A more recent wavefront shaping method that exploits only optical feedback is much more rapid [11]. Unfortunately, due to the location of the gain medium, the method is inherently limited to point-like (“single pixel”) imagery where only a small percentage of the light power is focused onto a point and more than 90% of the light is scattered to a broad background. Although a relatively high signal-to-noise ratio (SNR) can be obtained for an image of a single point, the SNR decreases linearly as the number of pixels increases, prohibiting the use for full-field imaging, see Appendix F and Ref. [8].

Here, we present an all-optical method for full-field imaging through thin scattering media in real time. It relies on a fundamentally different mechanism where the modes of a highly multimode laser cavity can phase lock onto a minimal loss state by passing only through uniform phase regions of the intracavity scattering medium, thereby minimizing scattering losses and ensuring high-quality imaging. We show that separating the gain medium from the scattering medium preserves all independent degrees of freedom of the highly multimode laser and significantly suppresses scattering. Moreover, since the gain medium is placed at the imaging plane of the object, our method allows high-quality and high-SNR imaging through thin scattering media, even for full-field imaging of complex objects.

The physical mechanism which enables imaging through scattering media inside a multimode laser cavity is inherently related to the process of mode buildup in lasers. In the pre-lasing stage, photons are spontaneously emitted from the gain medium and due to the random nature of the emission, a large ensemble of possible states (modes) is randomly sampled. These initial modes compete over the available gain, until only modes with minimal loss, and their coherent superposition, survive in the steady-state lasing stage [11,12]. Since a self-consistent laser mode must accurately retrace its path after a round trip in the laser cavity, the minimal-loss modes possess the intrinsic property of efficient self-imaging through the intracavity scattering media. When many such degenerate low-loss modes exist, their coherent superposition can well approximate an arbitrary image that would then be self-imaged inside the laser cavity.

Typical multimode laser cavities support only a small number of lasing modes (<100), and consequently are inadequate for optical imaging. Therefore, we resort to a highly multimode laser that supports >300 000 spatial modes, often referred to as a degenerate cavity laser or a self-imaging cavity laser [13–15]. When the numerical aperture (NA) of the laser cavity is larger than the diffusive angle of the scattering media, the laser selects the modes with minimal round-trip loss,

*sim.mahler@gmail.com

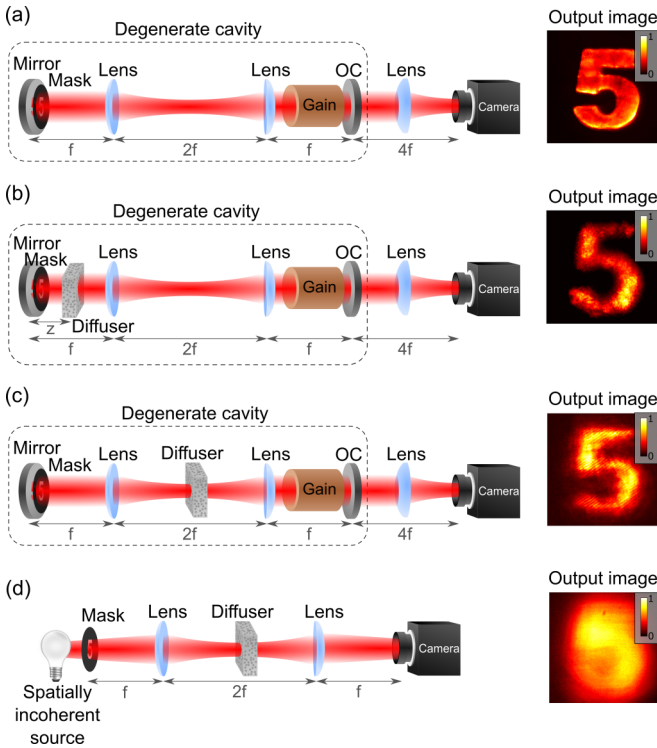


FIG. 1. Experimental arrangements for imaging through scattering media. (a) Imaging of a mask (object) in a degenerate cavity laser (DCL). The intensity distribution detected at the output plane (right inset) matches the shape of the object. (b) Imaging of a mask (object) in a DCL with an intracavity diffuser placed at distance $z = f/2$ from the object. The DCL overcomes the effect of scattering induced by the diffuser, so the intensity distribution at the output plane (right inset) still matches the shape of the object. (c) Imaging of a mask (object) in a DCL with an intracavity diffuser placed at the Fourier plane of the $4f$ telescope. (d) Imaging of a mask (object) with a passive $4f$ telescope (no optical feedback), where a diffuser is placed at the Fourier plane of the $4f$ telescope. Due to scattering induced by the diffuser, the detected intensity distribution (right inset) is smeared and the object cannot be identified. OC: output coupler.

which allow full-field imaging of the object. Due to the exponential buildup of the lasing modes [11,12], the time required for the laser to shape the beam traveling inside the cavity can be extremely short, on the order of several round trips [16,17]. Specifically, we show that the buildup time can be as short as 100 ns in a Q -switched laser, orders of magnitude faster than any other reported wavefront shaping method [18,19].

Our degenerate cavity laser (DCL) is comprised of an Nd:YAG gain medium, two flat mirrors and two lenses in a $4f$ telescope, f being the focal length of the lenses, Fig. 1(a). The $4f$ telescope assures that any field distribution is accurately imaged onto itself after a single round trip. Consequently, any transverse field distribution is an eigenmode of the cavity. Since all transverse modes supported by the cavity are loss-degenerate, they can all lase simultaneously, despite mode competition [11,13,15,17,20]. As the size of the exit pupil in a $4f$ telescope is much larger than its diffraction limit, the DCL supports many transverse modes. The $4f$ DCL is especially attractive as it enables physical access to both the position space (back mirror or output coupler planes) and k -space (Fourier

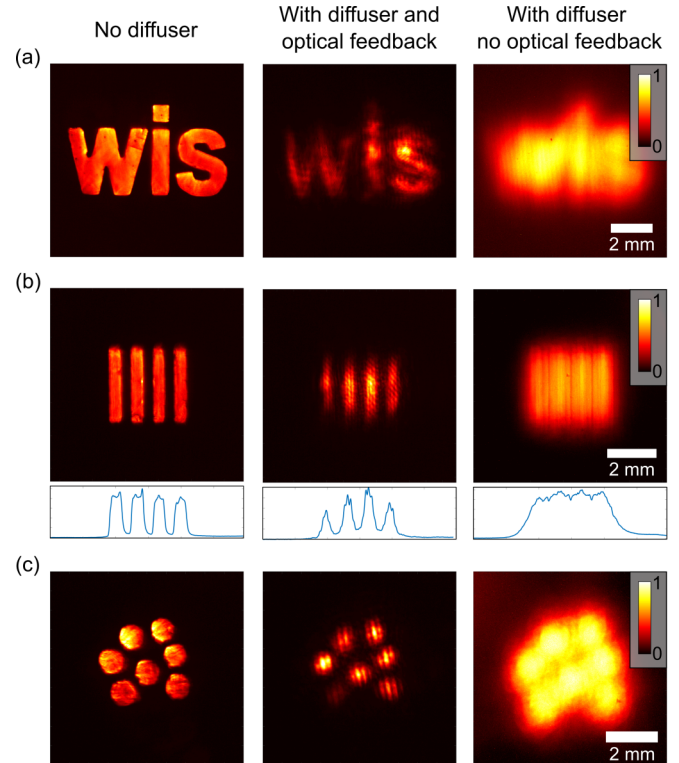


FIG. 2. Experimental results demonstrating intracavity imaging through scattering media for different objects. (a)–(c) Left column: Intensity distributions of the imaged objects at the output plane of a DCL with no diffuser [as in Fig. 1(a)]. Middle column: Intensity distributions at the output plane of a DCL, with a diffuser at the Fourier plane of the telescope [as in Fig. 1(c)]. Right column: Intensity distributions at the imaging plane of a passive $4f$ telescope (no optical feedback) with the same diffuser at the Fourier plane [as in Fig. 1(d)]. Bottom insets in (b) show cross sections of the intensity distributions. Panel (c) is the same as in (a,b), but here the middle column was obtained with a Q -switched cavity and a short 100-ns-pulse duration.

space, midway between the lenses) components of the lasing beam [1,21,22]. A detailed description of the experimental arrangement is included in Appendix A.

To demonstrate imaging through scattering media, a binary amplitude mask is placed near the back mirror of the DCL, serving as a reflective object, Figs. 1(a) to 1(c). When there is no optical diffuser inside the cavity, Fig. 1(a), the mask is imaged onto itself after every round trip, and therefore the lasing output beam is formed in the shape of the mask [23–25]. Surprisingly, when the diffuser is placed inside the cavity at a distance $z = f/2$, Fig. 1(b), the DCL is able to overcome the effect of scattering, and the image of the object is still clearly identified at the output plane of the laser. This is true also in the extreme case where the diffuser is placed at the Fourier plane of the $4f$ telescope, Fig. 1(c). For comparison, we also placed the object masks and the diffuser in an identical passive $4f$ telescope, Fig. 1(d). As expected, in this case the object cannot be identified. Figure 2 shows additional examples for objects being imaged through an optical diffuser.

As mentioned above, our method is extremely fast, and can acquire images in real time. To demonstrate such rapid

imaging through the scattering media, we Q -switched the DCL by placing a Pockels cell inside the cavity next to the back mirror. Figure 2(c) shows the experimental results with a Q -switched DCL where the lasing pulse duration was 100 ns. As evident, the Q -switched laser is able to image the object through the diffuser, despite the extremely short temporal duration of the lasing pulse.

To better understand the physical mechanism of our method, we focus on the extreme case where the diffuser is placed at the Fourier plane of the $4f$ telescope, as in Fig. 1(c) [see the discussion in Appendix B showing that the physical mechanism in this case is the same as that where the diffuser is placed before the lenses, as in Fig. 1(b)]. First, we compared the intensity distribution at the Fourier plane to the phase structure of the diffuser. Although the results of Fig. 1 were obtained with a generic diffuser, for simplicity, we start by considering a binary diffuser, namely a two-level optical diffuser inducing either 0 or π phase shifts to light propagating through it, Fig. 3(a).

Remarkably, when the binary diffuser is placed at the Fourier plane of the DCL [as in Fig. 1(c), but now with a binary diffuser], lasing occurs almost entirely at uniform phase regions of the diffuser, essentially eliminating the scattering induced by the diffuser, Figs. 3(a) to 3(c).

The reason for this effect can be readily understood by considering the round-trip field propagation of the cavity

$$E(\vec{x}, t + \tau_{\text{rt}}) = e^{g-\alpha} O(\vec{x}) \mathcal{F}^{-1} [D_{\text{rt}}(\vec{k}) \mathcal{F}[E(\vec{x}, t)]] e^{i\omega_0 \tau_{\text{rt}}},$$

where $E(\vec{x}, t)$ is the complex field at the plane of the object and transverse position \vec{x} and time t , τ_{rt} is the round trip time, g and α are the round trip gain and loss, $O(\vec{x})$ is the reflectance of the object, $D_{\text{rt}}(\vec{k}) = D(\vec{k})D(-\vec{k})$, where $D(\vec{k})$ is the phase transmittance of the diffuser at position \vec{k} in the Fourier plane of the $4f$ telescope, and ω_0 is the laser's natural frequency. Notice that the resonance condition for a standing wave requires that $\omega_0 \tau_{\text{rt}} = 2\pi n$, where n is an integer.

At threshold, the gain and loss are balanced, $e^{g-\alpha} \sim 1$, and a stable self-consistent mode, if it exists, is expected to return to itself after a single round trip, up to some global phase ϕ [12]. Therefore, we obtain

$$E_{\text{st}}(\vec{x})e^{i\phi} = O(\vec{x})\mathcal{F}^{-1}[D_{\text{rt}}(\vec{k})\mathcal{F}[E_{\text{st}}(\vec{x})]].$$

Clearly, a stable mode with low loss must be contained within $O(\vec{x})$. If $O(\vec{x})$ is a binary function, a trivial solution is obtained for $E_{\text{st}}(\vec{x}) \sim O(\vec{x})$ if $\mathcal{F}[E_{\text{st}}(\vec{x})]e^{i\phi} = D_{\text{rt}}(\vec{k})\mathcal{F}[E_{\text{st}}(\vec{x})]$, indicating that the field is transmitted through sufficiently uniform phase regions of the diffuser, thereby inducing an additional phase ϕ every round trip and pulling the laser's natural frequency to $\omega = \omega_0 + \phi/\tau_{\text{rt}}$. Indeed, Figs. 3(a) to 3(c) show that light is concentrated to uniform phase regions of the diffuser. If such a mode E_{st} exists, it would minimize round trip loss and consequently it will grow exponentially faster than any other mode [12]. If such a mode does not exist, the DCL would find a mode that approximates it. The ability of the DCL to well approximate the object $O(\vec{x})$, even with just a sparse representation in the Fourier plane, is related to the modal structure of the cavity, see Appendix E.

The fundamental limitation of our method is that the optical resolution of the intracavity $4f$ telescope must be high

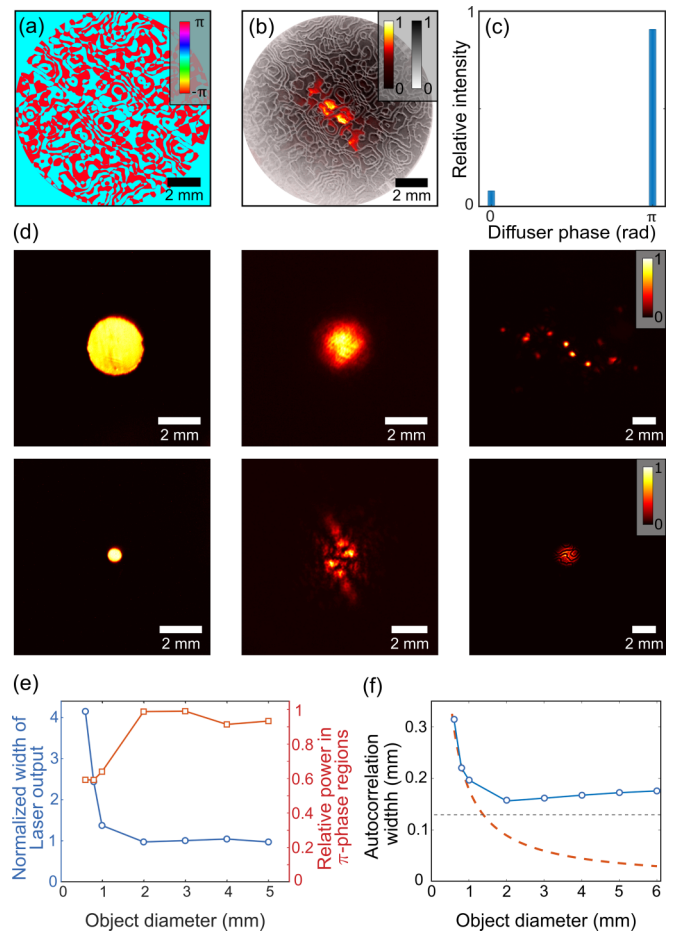


FIG. 3. Lasing through specific uniform phase regions of the binary diffuser. (a) Measured phase structure of the binary diffuser. (b) Lasing intensity distribution at the plane of the diffuser overlaid with the phase structure boundaries. (c) Relative lasing power in the 0 and π phase regions of the diffuser. (d) (left) Intensity distributions at the output plane of the DCL with no diffuser, as in Fig. 1(a), obtained with circular aperture objects of diameters $D = 2$ mm (top) and $D = 0.6$ mm (bottom). (middle) Intensity distributions at the output plane of the DCL with diffuser, as in Fig. 1(c), but with a binary diffuser. (right) Intensity distributions at the plane of the diffuser. (e) Width of the output beam normalized by the width of the object (blue circles) and relative lasing power in π -phase regions of the diffuser (red squares) as a function of the object diameter D . (f) Autocorrelation width of the intensity distribution at the plane of the diffuser [divided by $\sqrt{2}$] as a function of object diameter (solid blue), compared with the diffraction limit $\omega_0 = 0.42\lambda f/D$ (dashed red), and the effective size of a typical uniform phase region of the diffuser (dashed black).

enough to focus light to the small regions of uniform phase at the plane of the diffuser. This requires that the NA of the DCL must be large compared to the divergence angle of the optical diffuser. To verify this experimentally, we controlled the NA of the DCL by placing circular aperture objects with different diameters D near the back mirror, Figs. 3(d) to 3(f). As expected, only objects of large diameters (high NAs) were successfully imaged through the diffuser, Fig. 3(d). Specifically, Fig. 3(e), for objects of diameters $D < 2$ mm, the output beam was considerably larger than the object, and lasing

occurred through both 0 and π phase regions of the diffuser with approximately equal power. However, for $D > 2$ mm, the output lasing beam was comparable to the object in size and shape, and lasing occurred mostly through the π phase regions of the diffuser.

The failure of the laser to overcome the effect of the diffuser for small object diameters (small NAs) is clearly manifested by the lasing intensity distribution at the plane of the diffuser in Fig. 3(d) right column, and is inherently related to the modal structure of the laser cavity, see Appendix E. To show this more quantitatively, we calculated the autocorrelation width of the intensity distribution at the plane of the diffuser, Fig. 3(f). For a small object of $D < 2$ mm, the $1/e$ autocorrelation width is well approximated by the diffraction limit $\omega_0 = 0.42\lambda f/D$ of the $4f$ telescope, which exceeds the width of typical uniform phase regions on the diffuser.

For large objects of $D > 2$ mm, the width of typical lasing regions is approximately constant and barely changes with object size, demonstrating the strong tendency of the DCL to select and fill only regions of uniform phase. Accordingly, for large objects of $D > 2$ mm, the SNR in the images was above 100 (not shown).

Next, we placed in the intracavity Fourier plane a more general quasicontinuous optical diffuser (which was also used to obtain the results of Fig. 1), which consists of many random phase levels. The results are presented in Fig. 4. Figure 4(a) shows the experimentally measured phase-structure of the diffuser (see Appendix C), from which the phase gradient G was calculated. Figure 4(b) shows the overlay of the lasing intensity distribution at the plane of the diffuser and the phase gradient G . As is evident, lasing occurs in much smaller regions than those for the binary diffuser, Fig. 3(d) right column, and is limited to regions of low phase gradients, where scattering is minimized. Figure 4(c) shows this explicitly, by comparing the probability density distribution of the entire diffuser phase gradients $P(G)$ (solid black) and of the diffuser regions in which the lasing intensity is above 10% of its maximal value after basic noise reduction (dashed blue). Clearly, the distribution in regions with significant lasing is much narrower than that of the entire diffuser, and no lasing occurs in the high phase-gradients regions of the diffuser.

We also calculated the cross-correlation C between phase gradients G and intensity distribution I at the plane of the diffuser

$$C(\Delta r) = \frac{A \int G(r)I(r + \Delta r)d^2r}{\int G(r)^2d^2r \int I(r)^2d^2r} - 1, \quad (1)$$

where r is the position, Δr is a displacement in position and A is the area over which the integration is performed. We found that for $\Delta r = 0$, the intensity distribution is anticorrelated with the phase gradient, Fig. 4(d). This clearly indicates that lasing occurs only in regions of the diffuser with low phase gradients.

Numerical simulations of the multilevel diffuser further validate the results, Figs. 4(e) to 4(h). In particular, Fig. 4(g) shows that the simulated $P(G)$ of the entire diffuser is much broader than that of the regions with significant lasing, as in the experimental data in Fig. 4(c). For larger NA values, the DCL operation directs light to regions of low phase gradients, and consequently, the probability distribution is narrower.

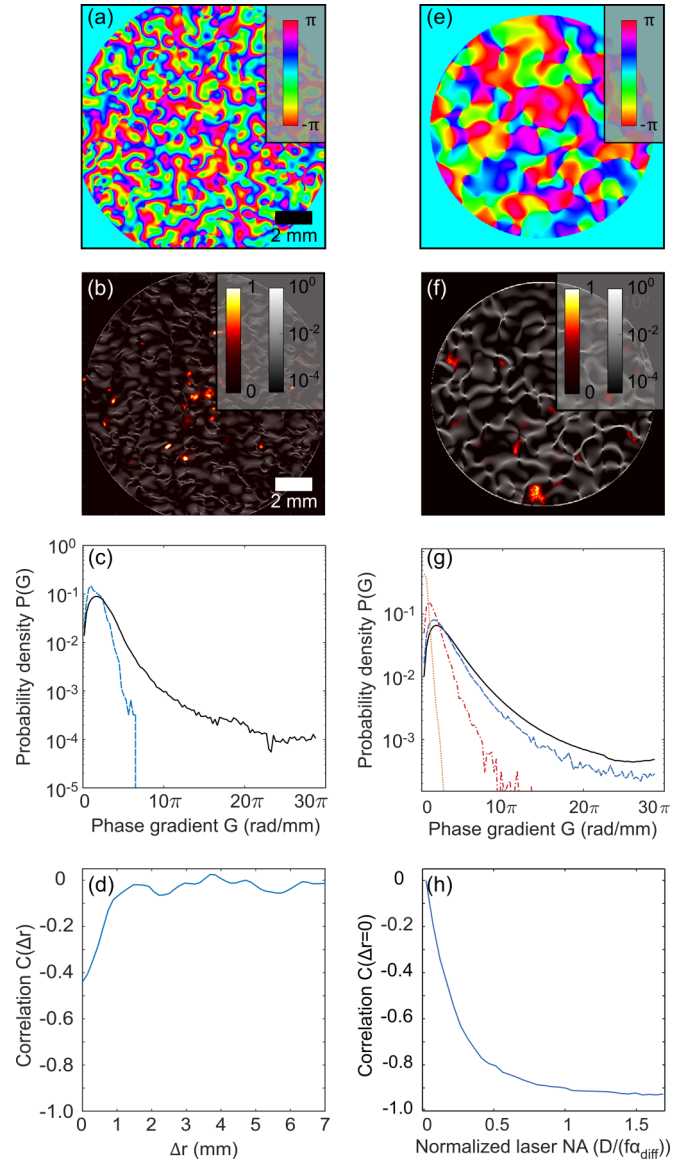


FIG. 4. Lasing through low phase-gradient regions of the intracavity diffuser. (a) Measured phase structure of the multilevel diffuser. (b) Absolute value of the phase gradient G , calculated from the phase structure in (a), overlaid with the measured lasing intensity distribution at the plane of the diffuser. (c) Probability density of phase gradients $P(G)$ of the entire diffuser (black) and of regions of the diffuser where the lasing intensity is $>10\%$ of its maximal value (dashed blue). (d) Cross-correlation $C(\Delta r)$ between the intensity distribution at the plane of the diffuser and the phase gradient $G(r)$. (e)–(h) Numerical results. (e) Simulated phase structure of the diffuser. (f) Phase gradient with lasing intensities. (g) $P(G)$ of the entire diffuser (solid black), and for regions where the lasing intensity is $>10\%$ of the maximal value for different normalized NAs of the intracavity telescope: 0.8 (dashed blue), 2 (dash-dotted red), and 6 (dotted yellow). (h) Cross-correlation peak C_0 as a function of the NA.

Figure 4(h) shows simulation results of the cross-correlation peak $C_0 \equiv C(\Delta r = 0)$ between the diffuser phase gradients and the lasing intensity distribution, as a function of NA. As is evident, for small values of NA the two are weakly

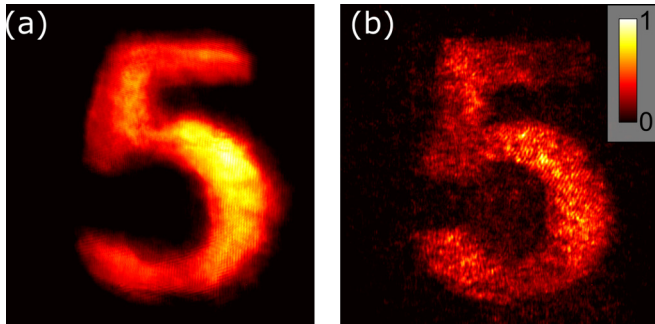


FIG. 5. Intensity distributions at the output plane of a DCL, with a diffuser at the Fourier plane of the telescope [as in Fig. 1(c)]. The diffusion angles of the diffusers used here were (a) 0.3° degrees and (b) 1° degree.

correlated ($C_0 \approx 0$). However, for larger values of NA they are anticorrelated (C_0 approaches -1).

The results so far were obtained with relatively weak optical diffusers, i.e., optical diffusers with a relatively small diffusion angle: Figs. 1 and 4 were obtained with an optical diffuser of a 0.2° diffusion angle (16 levels custom made HoloOr optical diffuser), and Figs. 2 and 3 were obtained with an optical diffuser of a 0.3° diffusion angle (binary custom made HoloOr DOE diffuser). However, as noted, our method also works with relatively strong optical diffusers, as long as the NA of the DCL is large compared to the diffusion angle of the diffuser. To show this, we placed a larger object (larger NA) behind the diffuser and compared the images obtained with optical diffusers with diffusion angles of 0.3° and 1° , Fig. 5. As is evident, with both diffusion angles the image can be clearly identified.

Finally, the needed threshold gain depends on several parameters, such as the scattering strength of the diffuser, geometric parameters of the DCL, and the shape and size of the imaged object. We measured the lasing pump threshold difference with and without a far-field diffuser in our DCL to be about 20%. A similar measurement was also made with a near-field diffuser in the DCL and the total output power changed by merely 15% [17,20].

To conclude, we demonstrated a different method for rapid full-field imaging through scattering media, using a highly multimode degenerate cavity laser and intracavity diffuser. In our method, the gain medium is placed at the imaging plane of the object, such that gain saturation enforces lasing of the entire imaged object. It does so by reconstructing an approximated image from a sparse representation in Fourier space, such that light is focused to relatively uniform phase regions on the plane of the diffuser. As compared to previous work [11], the location of the gain medium is crucial to enable full-field imaging through the scattering medium, see Appendix F. Note that the mask and back mirror could be replaced with a single reflective object and that our method applies also to cases where there are no optical elements between the object and the diffuser, as in Fig. 1(b). Therefore, the cavity can be realistically constructed around a reflective object hidden behind a scattering medium. In Appendix G we present two possible practical configurations.

We show that our method is applicable when the optical resolution of the intracavity telescope is sufficiently high in relation to the correlation length (i.e., minimal feature size) of the diffuser, so as to require careful and accurate optical design and alignment. Accordingly, we demonstrate our method, as a proof of concept, using thin optical diffusers with low diffusion angles. We believe there is no fundamental limitation and the method should work also for thin optical diffusers with large diffusion angles, as long as they are smaller than the NA of the DCL.

ACKNOWLEDGMENT

This work was supported by the Israel Science Foundation (ISF) (Grant No. 1881/17).

APPENDIX A: DETAILED EXPERIMENTAL ARRANGEMENT

The DCL in our experimental arrangement contained a Nd:YAG rod gain medium (wavelength $\lambda = 1064$ nm) of 9.5-mm diameter and 10.9-mm length that was pumped with long $100\text{-}\mu\text{s}$ quasi-continuous-wave (CW) pulses of a xenon flash lamp, at a slow repetition rate of 1 Hz, so as to minimize thermal lensing. The two lenses inside the cavity were antireflective (AR) coated plano-convex lenses, with diameters of $D = 50.8$ mm and focal lengths of 400 mm. The back mirror was a highly reflective mirror (reflectivity $R > 99.8\%$), and the output coupler was a partially reflective mirror ($R = 90\%$). All images were obtained using a standard triggered complementary metal oxide semiconductor (CMOS) camera (Ximea MQ013MG-E2). Two different optical diffusers were used. Figures 1 and 4 were obtained with a 16-levels custom made HoloOr optical diffuser, having a divergence angle of 0.2° degrees. Figures 2 and 3 were obtained with a binary custom made HoloOr DOE diffuser, having a divergence angle of 0.3° degrees.

1. Imaging through intracavity scattering media with a degenerate cavity laser

Figure 6 shows schematically the typical experimental arrangement of the degenerate cavity laser (DCL) with scattering media (intracavity diffuser) and the external detection configuration. The DCL is comprised of an Nd:YAG gain medium, two lenses of focal length $f = 400$ mm in a $4f$ telescope arrangement, a highly reflective back mirror, and a partially reflective output coupler. The object to be imaged was a binary amplitude mask placed adjacent to the back

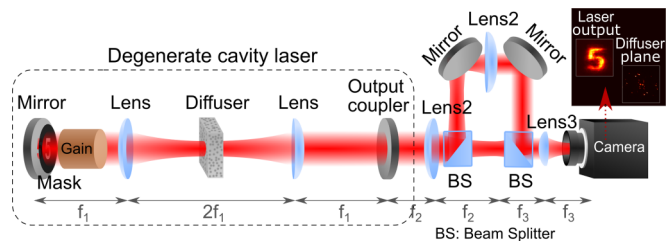


FIG. 6. Experimental arrangement of the DCL and the imaging system that was used for measuring the intensity distributions at the laser output plane and at the diffuser plane.

mirror and the optical diffuser (which served as the scattering media) was placed either in a midfield before the first lens, or at the Fourier plane between the two lenses of the $4f$ telescope. We noticed experimentally that the results are essentially the same when the gain medium is placed either near the back mirror or near the output coupler (not shown).

The telescope assures perfect imaging in the laser cavity whereby any field distribution is precisely imaged onto itself after a single round trip, and therefore any field distribution is an eigenmode of the cavity. Typically, the size of the exit pupil in the $4f$ telescope is much larger than the diffraction limit, so many transverse modes can all lase simultaneously. The DCL also has many different longitudinal modes, which are assumed to be uncorrelated with one another. The number of longitudinal modes in the cavity is estimated by the measured bandwidth of our laser (measured to be 30 GHz, not shown) divided by the spectral spacing between modes [$c/(2L) \approx 90$ MHz, where c is the speed of light, and L is the optical length the DCL], ~ 300 .

Outside the DCL, Fig. 6 (right), a beam splitter splits the laser beam light into two optical channels. The first channel images the intensity distribution at the output plane of the laser onto a camera, by means of Lens2 and Lens3. The second channel images the intensity distribution at the diffuser plane, by means of the intracavity Lens1, Lens2, Lens2, and Lens3, onto the same camera, but with a transverse shift as compared to the first channel. Accordingly, light from the two channels illuminate different regions of the camera. The camera, therefore, detects simultaneously the intensity distributions at both the output plane and at the diffuser plane. The focal distance of Lens2 was 200 mm and its diameter was 25.4 mm. The focal distance of Lens3 was 60 mm and its diameter was 25.4 mm.

2. Imaging through scattering media with a spatially incoherent source

Consider the case where the diffuser is placed at the Fourier plane [as in Fig. 1(c)]. Light from a coherent source that illuminates an object which contains only low spatial frequencies, would focus to a small spot. If the NA of the optical system is much greater than the diffusion angle of the diffuser, the size of the spot would be smaller than a typical flat region of the diffuser. Consequently, the image could be clearly viewed on the other side of the diffuser, even without optical feedback from the DCL. This is a trivial case, and not considered in our work.

If, however, the object contains higher spatial frequencies, the light will propagate through several phase regions at the Fourier plane, and therefore the image would be distorted. Generally, using light of spatially incoherent sources yields better imagery since some of the coherent noise artifacts are averaged out. For this reason, we evaluated our method by comparing our results to those obtained without optical feedback (i.e., outside the DCL) using a spatially incoherent source.

Figure 1(d) in the main text shows schematically the basic experimental arrangement for imaging through scattering media outside a laser cavity with a spatially incoherent source. The spatially incoherent source was obtained by illuminating

a fast rotating diffuser with a continuous wave Nd:YAG laser. The light from this source propagated through the object (a binary amplitude mask) and the output intensity distribution was then imaged through the scattering media and onto the camera using a $4f$ telescope configuration (the focal length of the telescope lenses was $f = 400$ mm and their diameters $D = 50.8$ mm).

APPENDIX B: IMAGING THROUGH THE DIFFUSER, WHEN PLACED BEFORE THE LENS

By placing the diffuser in a midfield between the object and the first lens, we demonstrate that our method is applicable even when there are no optical elements between the reflective object and the scattering media, as in Fig. 1(b). Figure 7 shows experimental results when the (multilevel) diffuser is placed at different axial midfield distances from the object (but before the first lens).

As evident in Figs. 7(a) to 7(f), the quality of the image is preserved and barely changes with the midfield distance z , when the diffuser is placed inside the DCL. We therefore conclude that our method is extremely robust and that the deleterious effects of the diffuser can be overcome, even when it is placed at various locations inside the cavity. For comparison, Figs. 7(g) and 7(h) show the noisy results when a diffuser is placed outside the DCL (no optical feedback), where the image degradation increases when increasing distance z between the object mask and the diffuser. [In this sense, the image would be distorted the most when the diffuser is placed at the far-field plane (“infinity”) or Fourier plane between the two lenses of the DCL].

In the main text, we explained mainly the effect of imaging through the diffuser when it is placed at the Fourier plane between the two lenses [the configuration in Fig. 1(c)]. We showed there that, if the laser light can propagate through regions of uniform phase at the plane of the diffuser, the field would be accurately imaged onto itself after every round trip, thus minimizing round trip loss. In full analogy to the formalism presented there, when the diffuser is placed before the lens, as in Fig. 1(b), the field distribution after a single round trip would be

$$E(\vec{x}, t + \tau_{rt}) = e^{g-\alpha} e^{i\omega_0 \tau_{rt}} O(\vec{x}) \times P_z[D(x)P_{-z}(P_{-z}\{D(\vec{x})P_z[E(\vec{x}, t)]\})],$$

where $E(\vec{x}, t)$ is the complex field at the plane of the object with transverse position \vec{x} and time t , τ_{rt} is the round trip time, g and α are the round trip gain and loss, $O(\vec{x})$ is the reflectance of the object, $D(\vec{x})$ is the phase transmittance of the diffuser at position \vec{x} and distance z from the object, ω_0 is the laser’s natural frequency, and $P_z[E(\vec{x}, t)]$ propagates the field $E(\vec{x}, t)$ a distance z , $P_z[E(\vec{x}, t)] = e^{ikz} \mathcal{F}^{-1}[\mathcal{F}[E(\vec{x}, t)] \exp(i\pi \frac{z^2}{\lambda z})]$.

If the field at the plane of the diffuser is confined to uniform phase regions of the diffuser, then D contributes only a global phase and the field is imaged onto itself after every round trip (up to the global phase). Imaging through the diffuser is therefore achieved if the laser distributes spherical-like phases to the light at the plane of the object $O(\vec{x})$ (the light must fill the object due to gain saturation), such that it will focus onto uniform phase regions of the diffuser.

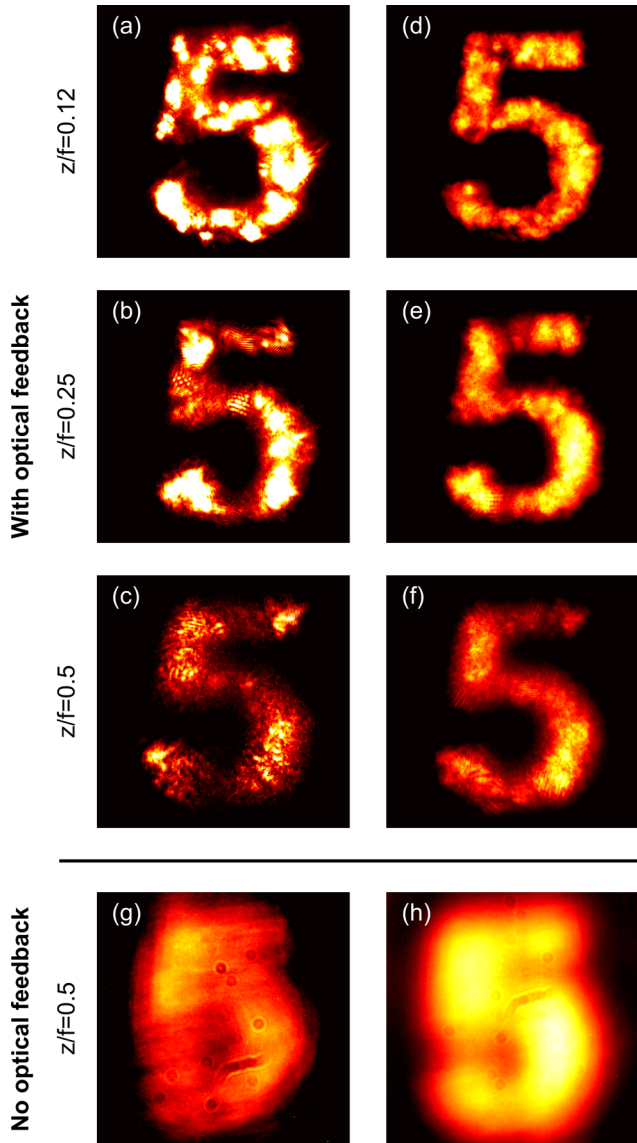


FIG. 7. Imaging through scattering media in the DCL, with no optical elements between the object and the scattering media. (a)–(c) Intensity distribution at the output plane of the DCL, when the multilevel diffuser was placed at various midfield distances from the object. (d)–(f) Same as (a)–(c), but here the the diffuser was slightly displaced transversely to obtain three different images which were then superimposed (averaging). The diffuser was placed at distance of (a), (d) $z/f = 0.12$ from the object, (b), (e) $z/f = 0.25$ from the object, and (c), (f) $z/f = 0.5$ from the object. For comparison, panel (g) shows the intensity distribution at the imaged plane of the object, when the diffuser is placed at $z/f = 0.5$ and when there is no optical feedback. (h) Same as (g), but when superimposing the detected results of three different locations of the diffuser. The focal distance of the two intra-cavity lenses was $f = 250$ mm.

APPENDIX C: PHASE-STRUCTURE MEASUREMENTS OF THE OPTICAL DIFFUSER

Figure 8 schematically presents the experimental arrangement and the Fourier processing procedure for measuring the phase structure of the optical diffuser, as in Figs. 3(a) and 4(a). The experimental arrangement, shown in Fig. 8(a), is a

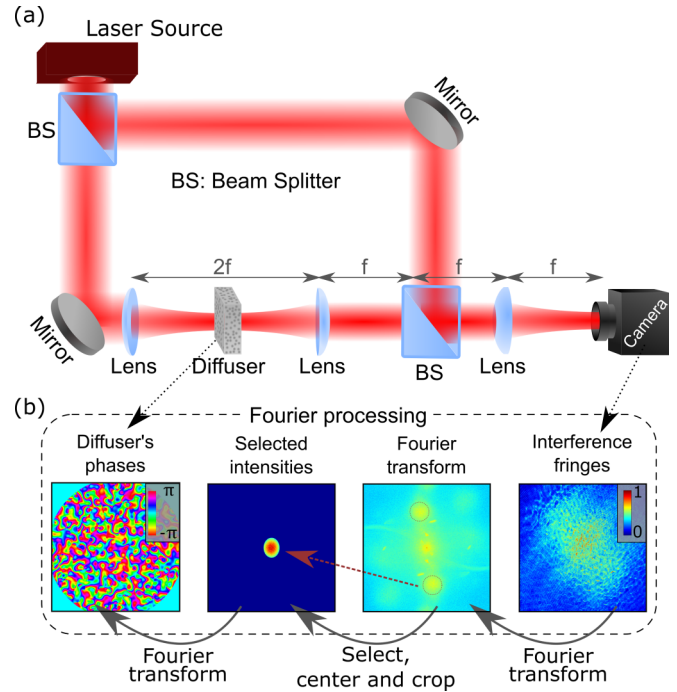


FIG. 8. Measurements of the diffusers' phase structure. (a) Experimental arrangement and (b) Fourier processing method used for measuring the phase structure of the optical diffuser.

Mach-Zehnder interferometer whose input is a relatively large diameter collimated light beam from a single-mode continuous wave 1064-nm laser.

The input laser light beam was divided by the first beam splitter into two light beams of equal intensities, so each propagates in a different channel. In the first channel, the light beam propagates through a telescope until the second beam splitter. The telescope is formed by two spherical lenses of focal length $f = 200$ mm and diameter $D = 50.8$ mm, and the diffuser was inserted midway between the two lenses, at the focal plane of the telescope. In the second channel, the laser light beam propagates in free space onto the second beam splitter with an angular orientation. At the second beam splitter plane, the two laser light beams interfere, forming interference fringes that are imaged to and recorded by a camera, Fig. 8(a), (right).

Figure 8(b) shows the Fourier processing procedure for determining the phase structure of the optical diffuser from the intensity distribution of the interference fringes (right image). First, the intensity distribution of the detected interference fringes was Fourier-transformed. Then an aperture was applied in Fourier space to select one of the two high-frequency lobes and move it to the center. Finally, an inverse Fourier transform is applied to obtain the phase distribution at the plane of the diffuser and thereby the phase-structure of the optical diffuser (left image). To compensate for aberrations and improve accuracy, we repeated the procedure after removing the diffuser and subtracted the resulting phase distribution at the plane of the diffuser from that with the diffuser.

It should be noted that when the diffuser is inside the DCL (see Fig. 6), light propagates through the diffuser twice every round trip, i.e., forward and backward directions. Due

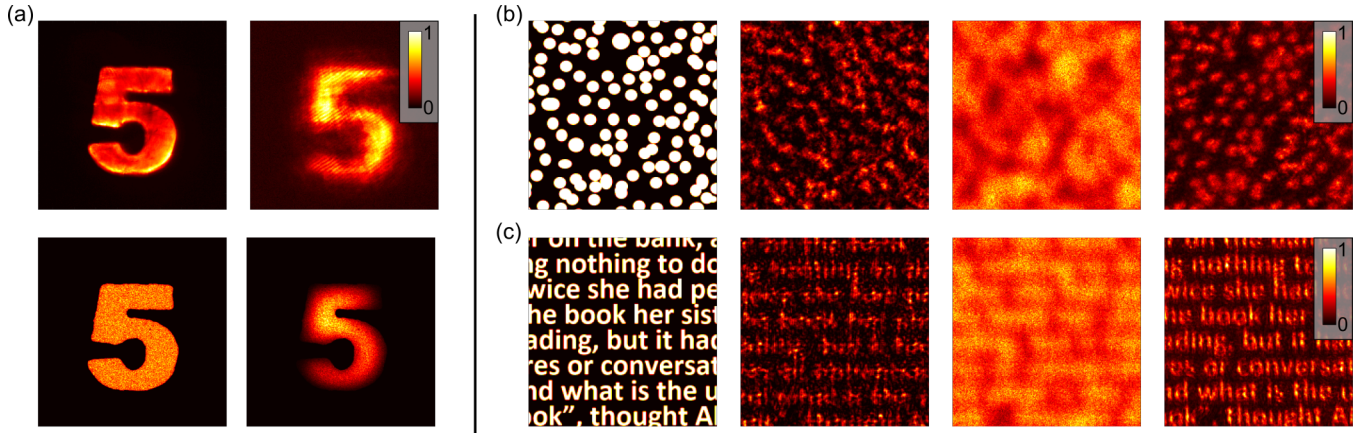


FIG. 9. Simulation results. (a) Comparison between experimental (top) and simulation (bottom) results. Left column: Experimental and simulated intensity distributions at the output plane of the DCL with no diffuser, as in Fig. 1(a); right column: Experimental and simulated intensity distributions at the output plane of the DCL with a diffuser inside the cavity, as in Fig. 1(c). (b), (c) Imaging of complex structures through scattering medium. Simulated intensity distributions at the output plane of the DCL, when a diffuser is placed at the Fourier plane inside the DCL, as in Fig. 1(c). First from left is the object; second from left is the simulated intensity distribution at the target’s imaging plane, when illuminating the object with a coherent plane wave with no optical feedback; Third from left is the simulated intensity distribution at the target’s imaging plane, when illuminating the object with incoherent light and with no optical feedback; Right is the intensity distribution at the target’s imaging plane, obtained with all-optical feedback.

to the inversion property of a $4f$ telescope, the field of one direction is rotated by 180° relative to the other direction. This 180° rotation effect was numerically taken into account in our measurements and analysis.

For the case of the binary diffuser, we compared the results of this method with those obtained by imaging the intensity distribution at the diffuser plane directly onto the camera, using a spatially incoherent source. As the binary diffuser is comprised of regions that induce 0 and π phase shifts, destructive interference occurs at the boundary between these regions, as seen in Fig. 3(b). Therefore, the different phase regions can easily be identified. We find that the results from this direct imaging method are in very good agreement with those from the more elaborate Fourier processing method of Fig. 8(b). Since it is simpler, cleaner, and less noisy, we mainly used the direct imaging method throughout our experiments for the binary diffuser in Fig. 3.

APPENDIX D: SIMULATION METHOD

The simulations presented in the main text are based on a Fox-Lee-type simulation, where the minimum loss eigenmode of the cavity is found by iteratively propagating a transverse field through the cavity, until a steady state is finally achieved. The transverse field is represented by a field matrix of $N \times N$ elements (pixels) and it is initially generated by distributing random phases and uniform intensity over all matrix elements. The optical components and propagation distances in the cavity are represented by a matrix, and therefore a single round trip in the cavity is represented by matrix multiplication. For the DCL, the propagation from the plane of one of the mirrors to the diffuser, and vice versa, is represented by a fast Fourier transform. After each round trip, the field is normalized, so as to account for loss and gain and avoid numerical instabilities.

Figure 9(a) compares simulated intensity distributions to those measured experimentally. In the simulations, the shape

of the object is the same as the physical mask that was placed inside the DCL, and the simulated diffuser has the exact same phase structure as the experimentally measured binary diffuser. The simulated results were obtained by summing the intensity distributions of 300 different simulations to account for the effect of the different longitudinal modes. To further demonstrate our method, we also simulate more complicated objects, as presented in Figs. 9(b) and 9(c). In these simulations, rather than normalizing the field every round trip (“cold-cavity”), the gain medium was taken into account by multiplying the field after every round trip by the gain matrix G ,

$$G_{i,j} = \frac{g_0}{1 + |E_{i,j}|^2/I_{\text{sat}}}, \quad (\text{D1})$$

where g_0 denotes the pump, $E_{i,j}$ denotes the field at pixel (i, j) and I_{sat} is the saturation intensity, and we assumed $I_{\text{sat}} = 2000$ and $g_0 = 3$. These images were obtained by summing the intensity distributions of 200 different simulations.

APPENDIX E: MODAL STRUCTURE

The ability of the DCL to image through scattering media is strongly related to the modal structure of the cavity, and a thorough understanding of such imaging can be obtained by analyzing the modal structure. For this purpose, consider a two dimensional DCL and a field vector E_{in} of n elements, which represents the field $E(x; z_0)$ at some initial plane z_0 inside the cavity. Each propagation distance and each optical element is represented in matrix form, and therefore a single round trip is represented by a single matrix M . Thus, the field E_{rt} after a single round trip is readily calculated by $E_{\text{rt}} = ME_{\text{in}}$.

If steady-state self-consistent modes are assumed, $E_{\text{rt}} = E_{\text{in}}$, the equation above reduces to an eigenvalue problem, where the eigenvectors represent eigenmodes of the

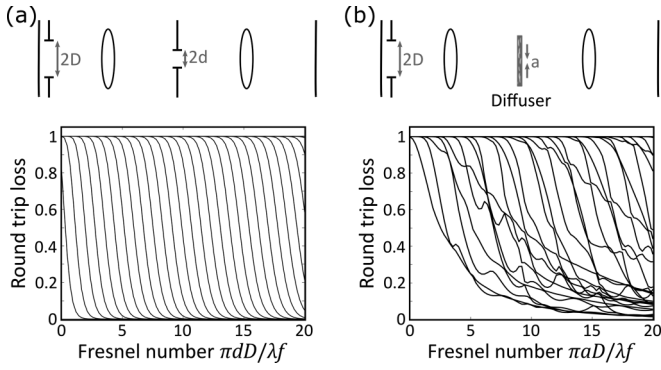


FIG. 10. Simulated modal structures of a degenerate cavity laser, showing round-trip loss as a function of Fresnel number. (a) Without an intracavity diffuser. (b) With an intracavity diffuser at the Fourier plane between the two lenses.

cavity and the eigenvalues are related to round-trip loss. We simulate a DCL with an aperture of varying diameter $2D$ near the back mirror and an aperture of diameter $2d$ in the Fourier plane between the two intracavity lenses.

Figure 10(a) shows the calculated loss as a function of the Fresnel number $\pi dD/(\lambda f)$ (λ being the wavelength and f the focal length of the lenses) for the lower-order modes, without an intracavity optical diffuser. As is evident, the modal structure is well ordered. As the size of the aperture is increased, there is a sharp decrease from high to zero loss for each mode. For large apertures, many modes have zero loss and are therefore loss degenerate. As a result, many modes can lase simultaneously, despite mode competition.

The number N of loss-degenerate modes, i.e., the number of expected lasing modes, depends on the ratio between the NA of the intracavity $4f$ telescope, D/f , and the divergence angle of the aperture at the Fourier plane, $\lambda/\pi d$, as follows:

$$N = \frac{\pi dD}{\lambda f} = \frac{D}{w_0}, \quad (\text{E1})$$

where $w_0 = \lambda f/\pi d$ is the size of a diffraction limited spot at the output plane of the DCL. In three dimensions, $N_T = N_x \cdot N_y$.

Figure 10(b) presents simulation results of round-trip loss as a function of the Fresnel number, with an optical diffuser inside the cavity. For objects with small aperture sizes, the numerical aperture of the cavity is small compared to the divergence angle of the diffuser, and therefore, the modes are highly lossy. As a result, imaging through scattering media cannot be achieved. However, for large objects, the numerical aperture of the cavity becomes large compared to the divergence angle of the diffuser, and therefore, there are many modes with low loss. For sufficiently large objects (i.e., sufficiently large NAs), the loss of many modes is close to zero, and therefore, many modes can lase simultaneously. The fact that the loss goes to zero implies that the modes are efficiently self-consistent, and therefore, can be used for imaging through the scattering media. Due to mode competition, modes with higher loss levels are not expected to lase.

The number of modes supported by the cavity N_{diff} is the ratio between the numerical aperture of the cavity and the

divergence angle $\alpha_{\text{diff}} = \lambda/(\pi a)$ of the diffuser

$$N_{\text{diff}} = \frac{\pi a D}{\lambda f} = \frac{D}{D_0}, \quad (\text{E2})$$

where a is the typical size of a single-phase region on the diffuser and $D_0 = \lambda f/\pi a$. In three dimensions, $N_T^{\text{diff}} = N_x^{\text{diff}} \times N_y^{\text{diff}}$.

Lasing through the scattering media is achieved when the round-trip gain overcomes the round-trip loss. Therefore, the plots in Fig. 10 also represent the required round-trip gain for a simple case of a one-dimensional (1D) object aperture. More generally, for an object that is imaged through a diffuser which is placed at the Fourier plane of the DCL, we estimate the minimal required round-trip gain by

$$g \sim \left(1 + \frac{A_{\text{diff}}}{A_{\text{obj}}}\right) \frac{1}{T_{\text{diff}}^2 R_{\text{OC}} R_{\text{obj}}}, \quad (\text{E3})$$

where A_{diff} and A_{obj} are the areas of the scattered light and object at the plane of the object, T_{diff} is the transmission of the diffuser, R_{obj} is the reflectivity of the object, and R_{OC} is the reflectivity of the output coupler, under the assumption of ideal transmission and collection of all other optical elements. For simple 1D apertures, $A_{\text{obj}} = f \times NA$ and $A_{\text{diff}} = f\theta_{\text{diff}}$, where f is the focal distance and θ_{diff} is the diffusion angle of the diffuser. Thus

$$g \sim \left(1 + \frac{\theta_{\text{diff}}}{NA}\right) \frac{1}{T_{\text{diff}}^2 R_{\text{OC}} R_{\text{obj}}}. \quad (\text{E4})$$

Since we require $NA > \theta_{\text{diff}}$, it is clear that the difference in the lasing pump threshold with and without a diffuser is small for diffusers of high transmission, $T_{\text{diff}} \sim 1$, as noted in the main text.

To verify our analysis in Eq. (E2) and simulation results, we placed circular apertures near the back mirror of the DCL and measured the number of lasing modes as a function of aperture size, when a binary optical diffuser was placed at the Fourier plane between the two lenses inside the cavity. The number of modes was measured by placing a second optical diffuser (Newport light shaping diffuser, 10° diffusion angle) outside the cavity and detecting the far-field intensity distribution with a camera. The number of modes N was estimated by the ratio of the standard deviation of the intensity distribution σ over the mean of the intensity distribution $\langle I \rangle$, as $N = \frac{\sigma}{\langle I \rangle}$.

Figure 11 shows the number of modes as a function of the aperture area. As is evident, for sufficiently large apertures, the number of modes grows linearly with the aperture area, in agreement with our conclusions above. The slope of the linear region is 0.91 mm^{-2} , which is close to the expected slope of 0.97 mm^{-2} .

Finally, it is constructive to establish an intuitive understanding of the relation between Figs. 10(a) and 10(b) in the language of modal phase locking. In the absence of the intracavity diffuser [Fig. 10(a)], there are many eigenmodes with equal (loss degenerate) eigenvalues. When a diffuser is placed inside the cavity [Fig. 10(b)] it couples between the different spatial modes, such that they can phase lock and consequently overcome the effect of the diffuser. Such phase locking is only possible when the detuning between modes is sufficiently small, as compared to the strength of coupling between them

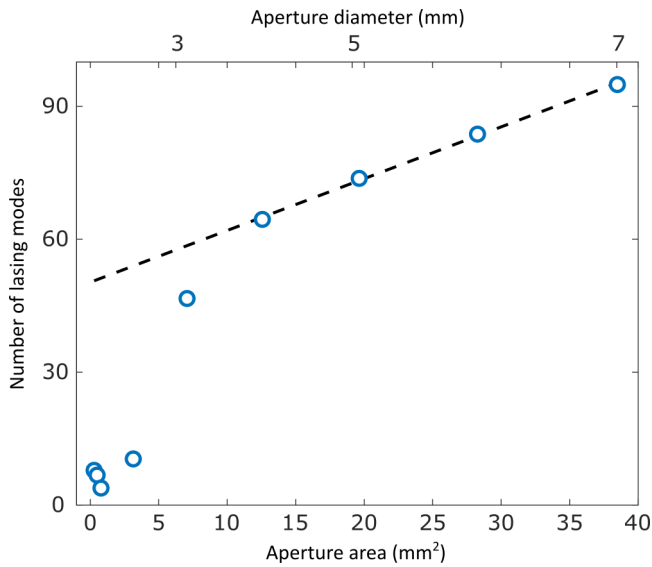


FIG. 11. Experimental measurements of the number of lasing modes as a function of aperture area (blue circles), together with a linear fit of the large aperture areas data points (dashed black line).

[26,27]. As a result, the modes are strongly detuned when lasing through regions of the diffuser that induce different phases, and therefore they cannot couple to one another and phase lock, and thus suffer from significant round-trip loss. To minimize loss, it is therefore preferable to lase through regions of equal phase, as indicated also by the analytic expressions in the manuscript. Indeed, in Fig. 3(c), >90% of the lasing power went through the π phase regions of the intracavity diffuser.

APPENDIX F: LOCATION OF THE GAIN MEDIUM

The gain medium can be located anywhere in the DCL, however, its location affects the lasing modes. In the following, we consider two possible locations of the gain medium: in the imaging plane of the object, as presented in the main text, and in the Fourier plane of the object (or near the diffuser) as in Ref. [11].

For the purpose of full-field imaging through a scattering medium, there are two significant advantages of placing the gain medium in the imaging plane of the object. First, the lasing modes tend to fill the object due to gain saturation, and consequently, full-field imaging can be achieved. If the gain medium is placed near the diffuser, the lasing modes tend to fill the diffuser and not necessarily the object. Therefore, even if the lasing modes overcome the scattering induced by the diffuser, they may not enable imaging of the *entire* object.

To demonstrate this, we simulated the DCL with an object near the back mirror and a diffuser at the Fourier plane of the $4f$ telescope; we also compared the lasing output when the gain medium is placed either at the imaging plane of the back mirror (near the object), Figs. 12(a) and 12(c), or at the Fourier plane (near the diffuser), Figs. 12(b) and 12(d). As is evident, when the gain medium is at the imaging plane of the object, lasing occurs through the entire object due to gain saturation and the object can clearly be identified, as in Fig. 12(c). However, when the gain medium is placed at the imaging

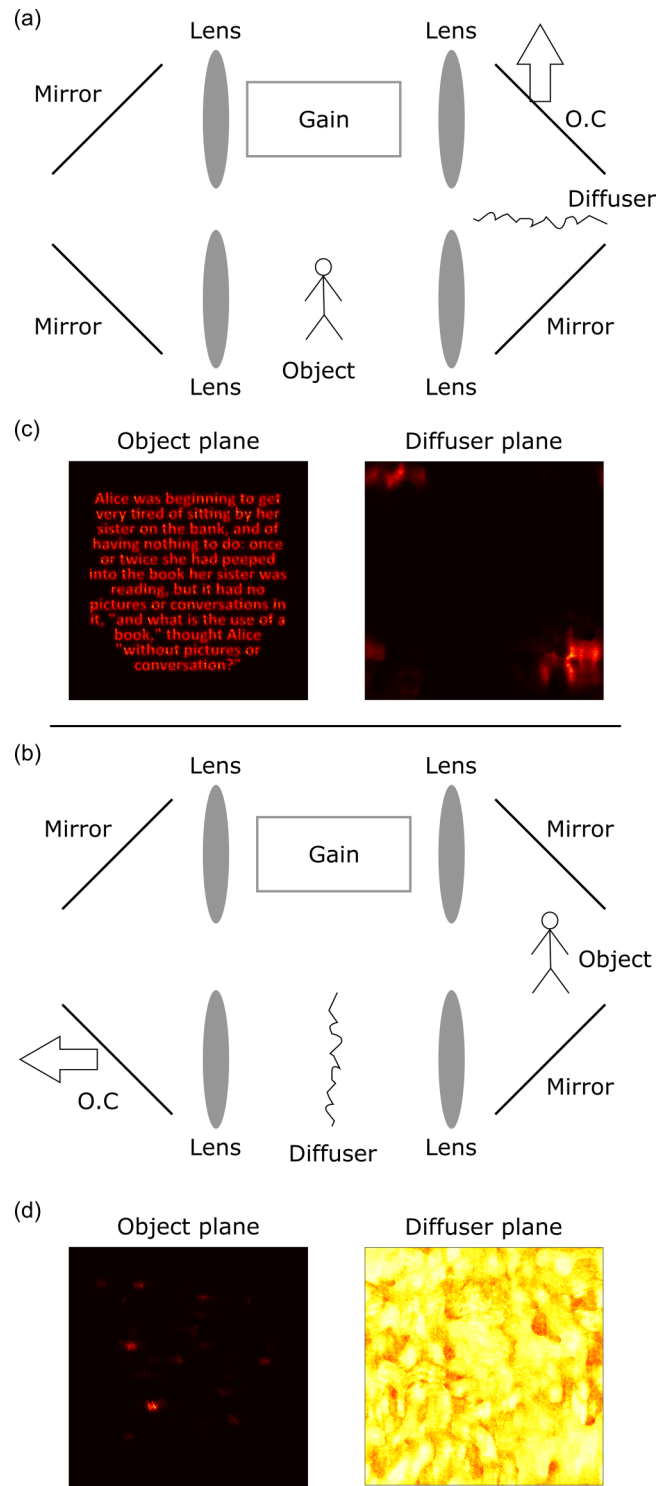


FIG. 12. Location of the gain medium. (a) Schematic diagram of the system simulated in (c), which is a ring DCL where the gain medium is placed at the imaging plane of the object. (b) Schematic diagram of the system simulated in (d), which is a ring DCL where the gain medium is placed at the imaging plane of the diffuser. (c), (d) Simulated intensity distributions at the imaging plane of the object (left) and of the diffuser (right).

plane of the diffuser, gain saturation guarantees lasing of the entire diffuser, not necessarily of the entire object. Accordingly, only a small portion of the object in Fig. 12(d)

lases, and the object cannot be identified. As predicted, only when the gain medium is placed at the imaging plane of the object can full-field imaging through the diffuser be achieved.

The second main advantage of placing the gain medium at the imaging plane of the object is that it improves the signal-to-noise ratio (SNR). As explained previously, the basic modes of the DCL are coupled to one another by the diffuser. If the detuning between the modes is small, they can phase lock to one another so as to minimize round trip loss, thereby enabling imaging of the hidden object. It should be noted that the number of modes that can phase lock determines the number of degrees of freedom in the DCL [11]. Therefore, as in standard methods of wavefront shaping, the SNR grows linearly with the number of degrees of freedom (i.e., the number of modes that can phase lock).

If the gain medium is placed at the imaging plane of the diffuser and if the gain medium is pumped sufficiently strongly, all regions of the diffuser participate in lasing due to gain saturation, as explained above. But since the optical path length through different regions of the diffuser differs substantially, many modes are highly detuned from one another, and consequently cannot phase lock. Therefore the number of modes that can phase lock in this case is small, and accordingly the SNR is low. On the other hand, if the gain medium is placed at the imaging plane of the object and if the pump is sufficiently strong, all regions of the object participate in lasing; at least in principle, all modes can couple to one another and propagate through equal-phase regions of the diffuser. Therefore, in this case, the number of modes that

can phase lock is high, and consequently the SNR would be high as well.

To verify this effect, we simulated a ring DCL, similar to that in Fig. 12, with a simple object of a small aperture and a diffuser and we compared the lasing output when the gain medium is placed either at the imaging plane of the object or at the imaging plane of the diffuser. As a function of pump power, we calculate the SNR, defined here as the ratio between the amount of energy inside the object to the total amount of energy outside the object, Fig. 13.

Indeed, as predicted, placing the gain medium at the imaging plane of the object significantly improves the SNR. Furthermore, when the gain medium is placed at the imaging plane of the object, the SNR drops much more slowly than in the case where the gain medium is placed at the imaging plane of the diffuser. Since, practically, in imaging systems it is preferable to work above threshold (different regions of the image may have different lasing thresholds, and since the pump is usually approximately uniform, the required pump is determined by the lowest lasing threshold in the image), there is a clear advantage to placing the gain medium at the imaging plane of the object.

APPENDIX G: PRACTICAL DESIGNS OF THE DCL

In this Appendix we briefly describe two possible configurations that could be used in practical applications. They incorporate the self-imaging properties and are similar to the DCL configurations that we investigated.

In the main text, we showed results for a linear DCL where the object was an amplitude mask that was placed near the back mirror of the DCL. Realistically, the object could be a reflective object, as illustrated in Fig. 14(a). Here the object must be specular and its reflectivity must be sufficiently high to overcome round-trip losses. Alternatively, a ring DCL could be built around an object placed between two optical diffusers, as in Fig. 14. Here the object is transmissive (or absorptive, and the image is detected as a negative of the object) and there are no optical elements between the object

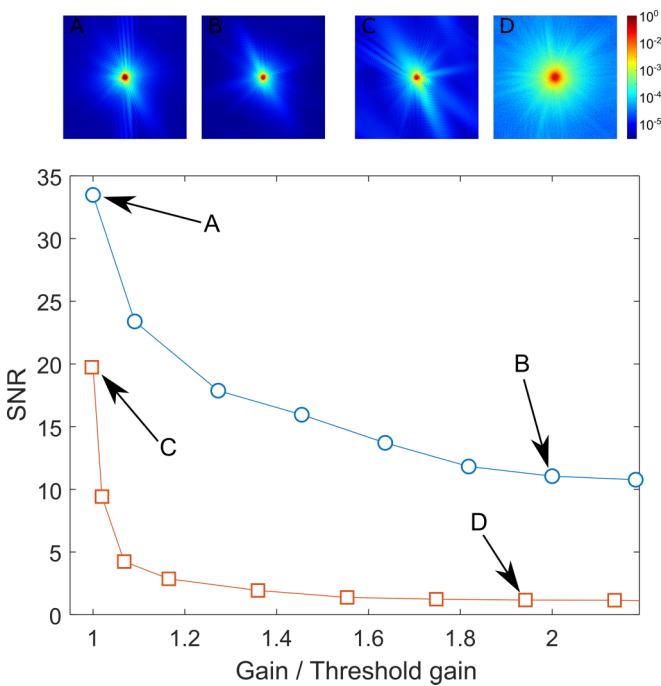


FIG. 13. Simulation results for signal-to-noise ratio (SNR) as a function of normalized gain for a small aperture object hidden behind scattering media, for the case where the gain medium is placed at the imaging plane of the object (blue circles) or at the imaging plane of the diffuser (red squares). Captions show simulated intensity distribution of the object (in log scale) at different points of the graph.

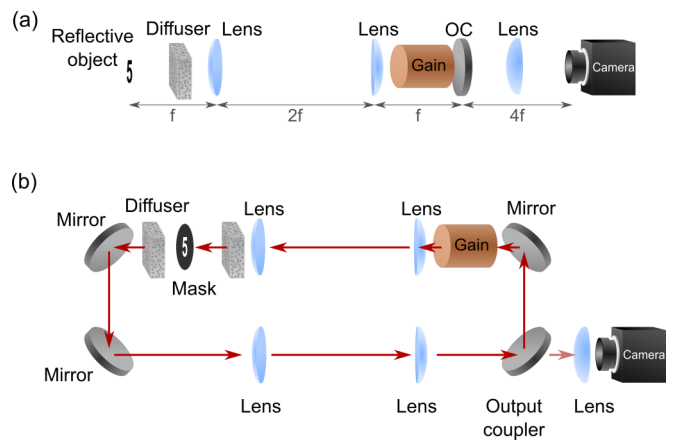


FIG. 14. Alternative design of the practical DCL arrangement for imaging through scattering media. (a) A linear DCL where the object is made of a specular object with sufficiently high reflectivity. (b) A ring DCL, where either the object is transmissive or absorptive (in which case a negative of the object will be obtained).

and the diffusive media. Note that while in a linear cavity light propagates through a single diffuser twice, in the ring cavity, we let the light propagate through two diffusive media. Since

the diffuser has a short correlation length, propagating twice through it is essentially the same as propagating once through two diffusers.

-
- [1] M. Nixon, B. Redding, A. A. Friesem, H. Cao, and N. Davidson, *Opt. Lett.* **38**, 3858 (2013).
- [2] R. Horstmeyer, H. Ruan, and C. Yang, *Nat. Photon.* **9**, 563 (2015).
- [3] S. Rotter and S. Gigan, *Rev. Mod. Phys.* **89**, 015005 (2017).
- [4] J. Bertolotti, E. G. van Putten, C. Blum, A. Lagendijk, W. L. Vos, and A. P. Mosk, *Nature (London)* **491**, 232 (2012).
- [5] O. Katz, P. Heidmann, M. Fink, and S. Gigan, *Nat. Photon.* **8**, 784 (2014).
- [6] E. Edrei and G. Scarcelli, *Optica* **3**, 71 (2016).
- [7] Z. Wang, X. Jin, and Q. Dai, *Sci. Rep.* **8**, 9088 (2018).
- [8] I. M. Vellekoop and A. P. Mosk, *Opt. Lett.* **32**, 2309 (2007).
- [9] O. Katz, E. Small, and Y. Silberberg, *Nat. Photon.* **6**, 549 (2012).
- [10] C. W. Hsu, S. F. Liew, A. Goetschy, H. Cao, and A. Douglas Stone, *Nat. Phys.* **13**, 497 (2017).
- [11] M. Nixon, O. Katz, E. Small, Y. Bromberg, A. A. Friesem, Y. Silberberg, and N. Davidson, *Nat. Photon.* **7**, 919 (2013).
- [12] A. E. Siegman, *Lasers* (University Science Books, Sausalito, CA, 1986).
- [13] D. Feldkhun, O. Tzang, K. H. Wagner, and R. Piestun, *Optica* **6**, 72 (2019).
- [14] J. A. Arnaud, *Appl. Opt.* **8**, 189 (1969).
- [15] H. Cao, R. Chriki, S. Bittner, A. A. Friesem, and N. Davidson, *Nat. Rev. Phys.* **1**, 156 (2019).
- [16] R. Chriki, S. Mahler, C. Tradonsky, V. Pal, A. A. Friesem, and N. Davidson, *Phys. Rev. A* **98**, 023812 (2018).
- [17] S. Mahler, Y. Eliezer, H. Yilmaz, A. A. Friesem, N. Davidson, and H. Cao, *Nanophotonics* **10**, 129 (2021).
- [18] A. Yariv and P. Yeh, *Photonics: Optical Electronics in Modern Communications* (Oxford University Press, New York, 2007).
- [19] O. Tzang, S. Labouesse, S. Singh, E. Niv, G. Myatt, and R. Piestun, in *Imaging and Applied Optics 2019 (COSI, IS, MATH, pCAOP)* (Optical Society of America, Washington, D.C., 2019), p. JTh3D.1.
- [20] Y. Eliezer, S. Mahler, A. A. Friesem, H. Cao, and N. Davidson, [arXiv:2109.04902](https://arxiv.org/abs/2109.04902).
- [21] A. Barthelemy, B. Colombeau, V. Couderc, A. Desfarges, O. Guy, V. Kermene, F. Louradour, and M. Vampouille, in *LEOS '95. IEEE Lasers and Electro-Optics Society 1995 Annual Meeting. 8th Annual Meeting. Conference Proceedings* (IEEE, New York, 1995), Vol. 2, pp. 192–193.
- [22] R. Chriki, M. Nixon, V. Pal, C. Tradonsky, G. Barach, A. A. Friesem, and N. Davidson, *Opt. Express* **23**, 12989 (2015).
- [23] R. Chriki, G. Barach, C. Tradonsky, S. Smartsev, V. Pal, A. A. Friesem, and N. Davidson, *Opt. Express* **26**, 4431 (2018).
- [24] W. A. Hardy, *IBM J. Res. Dev.* **9**, 31 (1965).
- [25] V. Couderc, O. Guy, A. Barthelemy, C. Froehly, and F. Louradour, *Opt. Lett.* **19**, 1134 (1994).
- [26] M. Fridman, M. Nixon, E. Ronen, A. A. Friesem, and N. Davidson, *Opt. Lett.* **35**, 526 (2010).
- [27] L. Fabiny, P. Colet, R. Roy, and D. Lenstra, *Phys. Rev. A* **47**, 4287 (1993).